

Chapter 2

Material Properties and Deposition Methods

The semiconductor compound CuInS_2 belongs to the family of I-III-VI₂ chalcopyrites. This chapter briefly summarizes the material properties of CuInS_2 and the related materials.

In the second part of the chapter, common techniques for the deposition of chalcopyrite thin films are briefly reviewed. Afterwards, the ion layer gas reaction (ILGAR) process is introduced, which constitutes an alternative to the established thin film deposition techniques. In particular, the Spray ILGAR process for the deposition of In_2S_3 thin films is explained, which served as a starting point for the development of a deposition process for CuInS_2 thin films in the framework of this thesis.

2.1 Material Properties

This section briefly summarizes the fundamental structural properties of CuInS_2 (section 2.1.1.). Subsequently, the phase relations and lattice defects in the ternary Cu-In-S materials system are discussed (section 2.1.2.). Also the properties of the binary material systems Cu-S, In-S and In-O are considered (section 2.1.3.), since they are known to play a major role in the growth of CuInS_2 thin films. Since this thesis focuses on the crystalline and structural properties of CuInS_2 thin films as well as on their growth process, only these properties are discussed. For a survey of the electronic properties of CuInS_2 , the reader is referred to Ref. [Jaffe '83; Jaffe '83; Jaffe '84; Alonso '01; Lazewski '02].

2.1.1. Structural Properties of CuInS_2

First reports about CuInS_2 date back to 1953, in which Hahn *et al.* [Hahn '53] analyzed the crystal structure of several ternary polycrystalline chalcopyrite materials, including CuInS_2 , by X-ray diffraction. In the following years, the properties of CuInS_2 single crystals were investigated by Tell *et al.* [Tell '71; Tell '74]. In 1975, Kazmerski *et al.* [Kazmerski '75] prepared the first CuInS_2 thin films exhibiting both p- and n-type conductivity. Due to their direct band gap of 1.52 eV and a high absorption coefficients of about 10^5 cm^{-1} in the visible range of the solar spectrum, CuInS_2 thin films attracted increased interest as a possible absorber material in solar cells [Kazmerski '75; Neumann '81].

Based on data obtained by density-functional theoretic calculations, Jaffe and Zunger [Jaffe '83; Jaffe '83; Zunger '83; Jaffe '84] gave a comprehensive summary of the electronic and optical properties of various chalcopyrite compounds, including CuInS_2 . These reports provided a profound theoretical basis for further studies of chalcopyrite materials for solar cell applications.

As already mentioned, CuInS_2 is a semiconductor belonging to the group of materials that exhibit a chalcopyrite-like structure with a composition of I-III-VI₂, where I is Cu or Ag, II is

Al, Ga, In, Tl, and III is S, Se, Te and I, III and VI indicate the group of the elements in the periodic system [Hahn '53; Goodman '54]. This group of materials has been named after the mineral chalcopyrite (CuFeS_2). The chalcopyrite structure can be deduced from the diamond structure according to the Grimm-Sommerfeld-rule, which states that a tetragonal structure is formed, if the average number of valence electrons per atom equals four [Grimm '26]. This deduction is visualized in Fig. 2.1a. In Fig. 2.1b and c the zincblende and chalcopyrite structure are depicted.

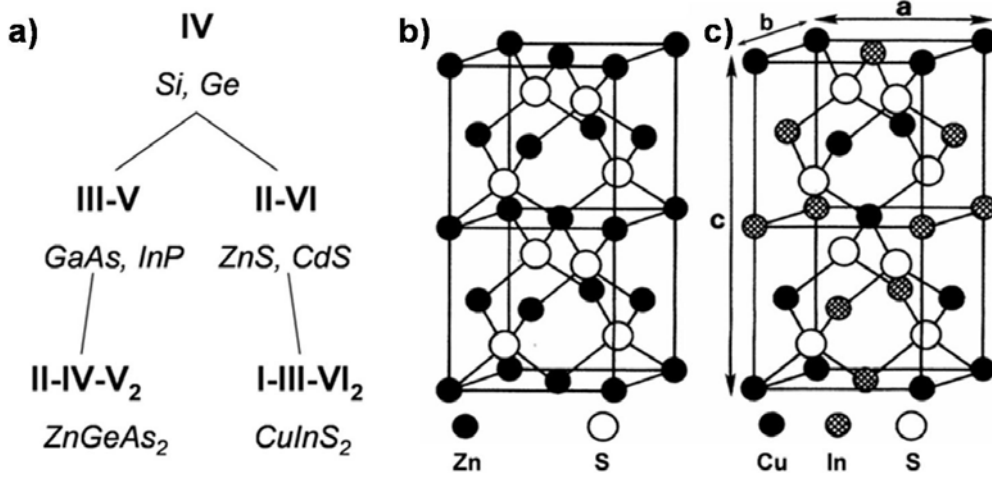


Fig. 2.1: a) Deduction of the chalcopyrite structure from the diamond structure according to the Grimm-Sommerfeld-Rule including exemplary compounds [Grimm '26]; b) and c) schematic sketch of the zincblende (ZnS) and chalcopyrite (CuInS₂) structure, respectively [Jaffe '84]

It can be seen that the chalcopyrite structure follows from the zincblende structure, if one half of the cations (Zn) are replaced by copper and the other half by indium atoms. The sulfur atoms remain unchanged in the same position. However, due to the two different kinds of atoms occupying the cation sites, the lattice is slightly distorted, so that the interatomic distances between the anion C and the respective cations A and B are in general no longer equal in the chalcopyrite structure. For I-III-VI₂ semiconductors, this so-called *tetragonal distortion* can be quantified by the parameters η_{tet} and u , with

$$\eta_{\text{tet}} = \frac{c}{2 \cdot a} \text{ and } u = 0.25 + \frac{R_{\text{II-III}}^2 - R_{\text{I-III}}^2}{a^2} \quad \text{Eq. (2.1)}$$

Here, $R_{\text{II-III}}$ and $R_{\text{I-III}}$ are the distances between the corresponding I-, II-, and III-atoms in a I-III-VI₂ compound. In Fig. 2.2., the parameters η_{tet} and u are shown graphically for CuInS₂. In Table 2.1, values for a , c , η_{tet} and u are listed for some chalcopyrites as reported in Ref. [Hahn '53; Jaffe '84].

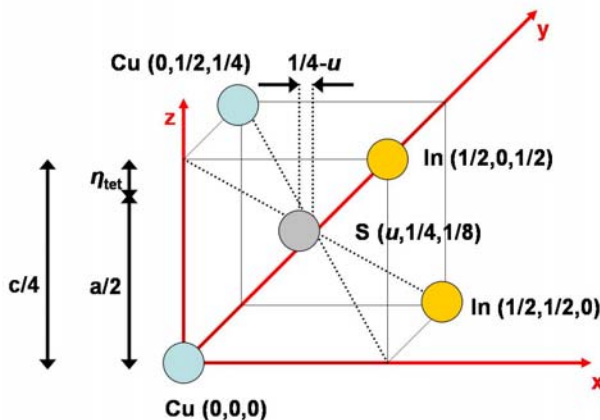


Fig. 2.2: Visualization of the parameters η_{tet} and u that characterize the tetragonal distortion of the chalcopyrite lattice. The atomic lattice positions are given in units of the lattice constant a .

Table 2.1: Atomic distances a and c and tetragonal distortion parameters η_{tet} and u for some chalcopyrite-type compounds (CuInS_2 , CuInSe_2 , CuGaSe_2) as reported in Ref. [Hahn '53; Jaffe '84]

	a [Å]	c [Å]	η_{tet}	u [a]
CuInS_2	5.517	11.118	1.0025	0.20
CuInSe_2	5.773	11.55	1.0005	0.22
CuGaSe_2	5.607	10.99	0.9800	0.25

Due to the tetragonal distortion, chalcopyrite-type and zincblende-type compounds belong to different space groups. The primitive unit cell of the chalcopyrite structure contains two formula units I-III-VI₂ ($2 \times 4 = 8$ atoms) and belongs to the space group I-42d, whereas in the zincblende structure, the primitive unit cell only contains two atoms and is assigned to the space group F-43m.

As a consequence of the Grimm-Sommerfeld-rule, it is possible to replace a certain portion of an atomic species by another isovalent species without giving up the chalcopyrite structure of the material, e.g., indium can be replaced by gallium in CuInS_2 . Thus, chalcopyrites can form a large variety of alloys. For example, the chalcopyrite solar cell absorbers yielding the best efficiencies to date, consist of $\text{Cu}(\text{In,Ga})\text{Se}_2$, i.e. CuInSe_2 , in which indium was partially replaced by gallium [Repins_1 '08]. In general, the group of chalcopyrite-type compounds, which are relevant for photovoltaic applications can be summarized as $\text{Cu}(\text{In,Ga})(\text{S,Se})_2$ or $\text{CuIn}_{1-x}\text{Ga}_x\text{S}_{1-y}\text{Se}_y$, with $0 \leq x, y \leq 1$.

2.1.2. Phase Relations and Defects

The growth behavior of compound materials is strongly influenced by the variety of existing phases that can be formed by the elements present during the growth process. For ternary compounds such relations can be described by a Gibbs phase triangle, which depicts the equilibrium phases that can be formed from the three elements at a certain temperature and pressure. Here, the three elements are located on the corners of the triangle and their binary compounds are projected on the edges. Inside the triangle, the ternary compounds are positioned according to their stoichiometry. Such a Gibbs phase triangle is shown in Fig. 2.3 for the system Cu-In-S at room temperature and normal pressure. For the sake of simplicity, only those binary compounds are depicted, which are most relevant for this thesis. A complete Gibbs phase diagram including all binary phases can be found in Ref. [Lewerenz '04].

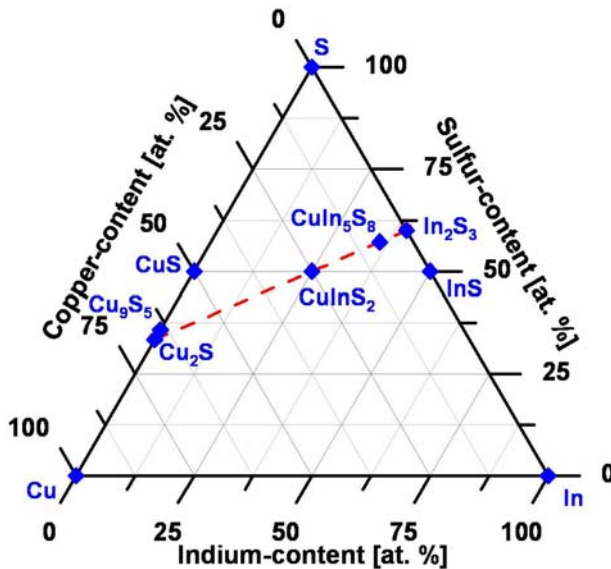


Fig. 2.3: Gibbs phase triangle at room temperature and normal pressure for the Cu-In-S system. The Cu_2S - In_2S_3 tie line is indicated by the dashed line. The three elements copper, indium and sulfur are located at the corners of the triangle. Of the binary phases, the compositions of In_2S_3 , InS , CuS , Cu_9S_5 and Cu_2S are marked. Additionally, the only stable ternary phases CuInS_2 and CuIn_5S_8 are marked.

As can be seen from Fig. 2.3, CuInS_2 is located on the Cu_2S - In_2S_3 tie line. Along such a quasibinary tie line, the homogeneity regions of the respective compounds can be analyzed as

a function of temperature. In the following, the quasibinary phase diagram of the Cu_2S - In_2S_3 tie line is discussed. The binary phase diagrams of Cu - S and In - S are discussed in the next section (section 2.1.3). For a discussion of the quasibinary CuS - InS phase diagram, the reader is referred to the work of Fiechter *et al.* [Fiechter '98].

The quasibinary phase diagram of Cu_2S and In_2S_3 shows the homogeneity regions and stable phases for different ratios of Cu_2S and In_2S_3 as a function of temperature. In Fig. 2.4., this diagram is shown as reported by Binsma *et al.* [Binsma '80] for normal pressure (1013 mbar).

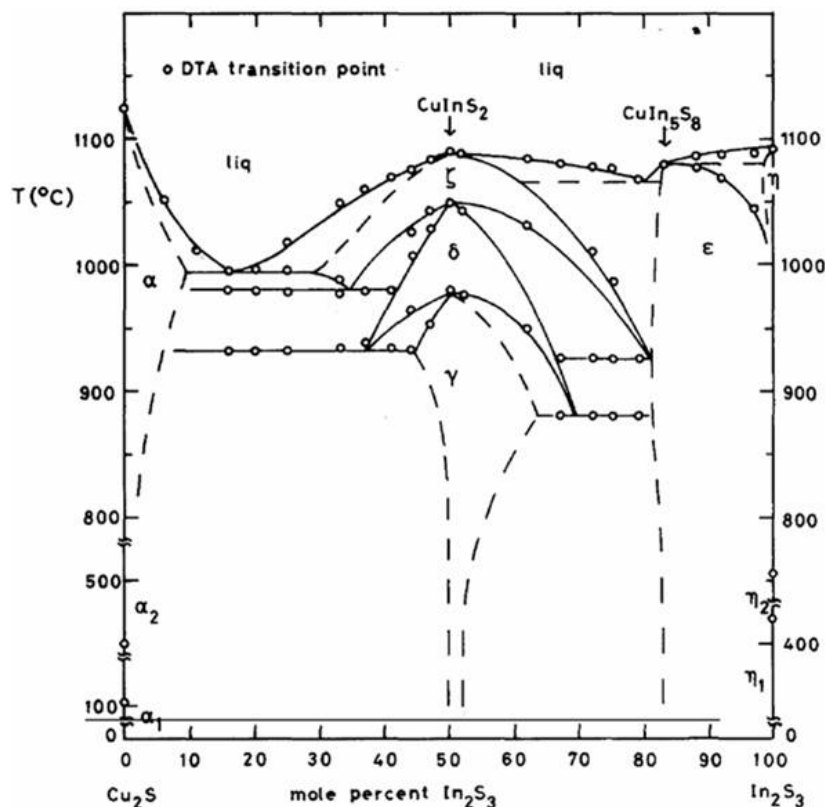


Fig. 2.4: Quasibinary phase diagram for the Cu_2S - In_2S_3 tie line of the ternary Cu - In - S phase diagram at normal pressure (1013 mbar) as reported by Binsma *et al.* [Binsma '80]. The stability regions of the three CuInS_2 modifications are marked with γ , δ , and ζ . ϵ stands for CuIn_5S_8 , whereas α_1 , α_2 , and α_3 are the different phases α - Cu_2S , β - Cu_2S and $\text{Cu}_{2-\delta}\text{S}$. η_1 , η_2 and η_3 stand for the three In_2S_3 modifications. (section 2.1.3)

From Fig. 2.4, it can be seen that besides the binary phases, CuIn_5S_8 and CuInS_2 are the only stable ternary phases in the Cu_2S - In_2S_3 quasibinary phase diagram. Both are stable at room temperature. For CuIn_5S_8 (ϵ in Fig. 2.4; space group F-43m) the spinel-ordered phase is the only known solid phase, which is stable until the melting point of 1085 °C is reached [Binsma '80]. In contrast, CuInS_2 can exist in three stable modifications. Below a temperature of 980 °C, CuInS_2 exists in the chalcopyrite structure (γ in Fig. 2.4; space group I-42d). Between 980 °C and 1045 °C CuInS_2 forms the sphalerite structure (δ in Fig. 2.4; space group F-43m), in which the copper and indium atoms are statistically distributed on the cation sites of the lattice, which leads to an elimination of the tetragonal distortion of the unit cell [Binsma '80]. Another CuInS_2 phase of unknown structure is reported for the temperature range between 1045 °C and the melting point 1090 °C (ζ in Fig. 2.4).

In this work only temperatures of up to 550 °C were used. Thus, only chalcopyrite-type CuInS_2 should be observed. However, also metastable phases might exist. In Fig. 2.5, three possible CuInS_2 structures are shown, which fulfill the Grimm-Sommerfeld rule [Wei '99].

In Fig. 2.5a the so-called “*CuPt cation-ordered*” (CuPt -ordered) structure is shown, which can be deduced from the I-III-VI₂ chalcopyrite structure (Fig. 2.5b) by occupying the cation sites in the [111] directions by alternating layers of I- and III- atoms. This structure can be assigned to space group R-3m. The structure in Fig. 2.5c is called “*CuAu I-type cation-ordered*” (CuAu -ordered). It follows from the chalcopyrite structure, if alternating layers of I- and III- atoms occupy the cation sites in the [100] directions. The space group of the CuAu -ordered structure is P-4m2. Both phases are named after the superlattices observed in the respective

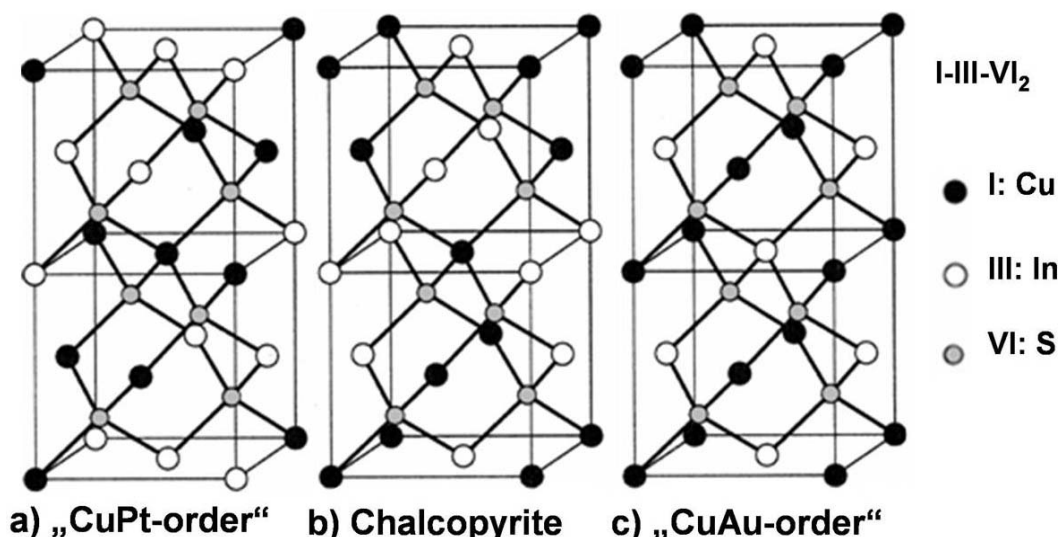


Fig. 2.5: Possible metastable phases of nominal CuInS₂ compounds, which fulfill the Grimm-Sommerfeld rule: a) CuPt-ordered structure; b) Chalcopyrite structure; c) CuAu-ordered structure [Wei '99].

metal alloys CuPt and CuAu. Wei *et al.* [Wei '99] calculated the formation energies of these phases for a transition from the chalcopyrite structure by density functional theory for various I-III-VI₂ compounds, including CuInS₂. For CuInS₂ they calculated formation energies of 8 meV per formula unit (4 atoms) for the CuAu-ordered phase and 213 meV per formula unit for the CuPt-ordered phase. Due to the low formation energy the existence of CuAu-ordered CuInS₂ seems possible at room temperature, whereas the presence of the CuPt-ordered phase of CuInS₂ is unlikely. CuAu-ordered CuInS₂ has been observed by different authors [Su '98; Alvarez-Garcia_1 '01; Alvarez-Garcia '02; Riedle '02; Rudigier_1 '04; Alvarez-Garcia '05]. In particular, a strong contribution of this phase was observed for epitaxial CuInS₂ films grown on Si(100) substrates [Su '98; Alvarez-Garcia '02], but it was also observed in polycrystalline thin films grown under copper-poor conditions or at low temperatures ($T < 500$ °C) [Riedle '02; Rudigier_1 '04].

Besides these metastable phases, point defects also exist in the lattice of CuInS₂. For CuInS₂, twelve intrinsic defects are possible: three vacancies (V_{Cu} , V_{In} , V_S), three interstitials (Cu_i , In_i , S_i) and six antisite positions (Cu_{In} , Cu_S , In_{Cu} , In_S , S_{In} , S_{Cu}) of copper, indium and sulfur. Here, the symbol represents the species present (V is a vacancy) and the index the species which occupies the same position in the perfect lattice. The occurrence of these defects in the actual CuInS₂ lattice will depend on their enthalpy of formation. The latter has been calculated for the intrinsic defects of CuInS₂ and CuInSe₂ by different authors [Neumann_1 '83; Neumann_5 '83; Ueng '87; Ueng '89; Fiechter '00]. From these values it can be concluded that anion-cation antisite defects can be excluded due to high enthalpy values. In contrast, copper vacancies were proposed to be the most frequent defect in CuInS₂ (concentration about 10^{19} - 10^{20} cm⁻³; [Ueng '89]). Since the copper vacancy acts as an acceptor, it also determines the dopant concentration and p-type conductivity of CuInS₂. Additionally, it was proposed that these defects interact with each other by forming charge-neutral defect pairs. Besides their electronic properties as acceptors or donors, the intrinsic defects also play an important role in the growth process of CuInS₂ thin films, since especially vacancies provide diffusion paths and can thus favor the diffusion of a certain species.

2.1.3. Secondary Phases

In this section, the structural properties and stable phases of the binary Cu-S, In-S and In-O material systems are reviewed. Since such binary phases were observed as secondary phases during the growth process of Spray ILGAR CuInS₂, their properties are likely to influence the

growth process. Oxygen is considered because of the use of oxygen-containing solvents. It will be shown, however, that no Cu-O phases are involved. Therefore, the latter are not discussed. The binary phase diagrams of these systems are shown in Appendix IV.

The Cu-S Material System

The binary phase diagram of the Cu-S material system is shown in Appendix IV (Fig. IV.1). In this material system a large variety of compounds has been reported [Massalski '90]. At room temperature and normal pressure (1013 mbar) CuS (covellite), α -Cu₂S (α -chalcocite), Cu_{1.96}S (djurlite) and Cu_{1.75}S (anilite; also written as Cu₇S₄) are stable. At about 100 °C β -Cu₂S (β -chalcocite) and Cu_{2- δ} S (digenite including Cu₉S₅) become stable. Even though they exhibit different crystal structures (Table 2.2), besides CuS, all these compounds have [Cu]:[S] ratio of about two. Besides these stable phases various metastable phases are known [Massalski '90]. Since the metastable phases were not observed in the course of this thesis, they are not listed in Table 2.2. All copper sulfides are degenerate p-type semiconductors with low thermal activation energies for conductivity (<0.6 eV) [Landolt '08].

Table 2.2: Stable copper sulfide phases in the Cu-S material system at normal pressure (1013 mbar) for the relevant temperature range of this thesis (25 °C ≤ T ≤ 550 °C). The stability range, [Cu]:[S] ratio and space group are listed for each phase according to Ref. [Massalski '90] and [Landolt '08].

	Name	Stability Range at 1013 mbar	[Cu]:[S]	Space group	Reference
CuS	Covellite	T ≤ 507 °C	1	P6 ₃ /mmc	[Landolt '08]
α -Cu ₂ S	α -chalcocite	T ≤ 103 °C	2	P2 ₁ /c	[Landolt '08]
β -Cu ₂ S	β -chalcocite	103 °C ≤ T ≤ 437 °C	2	P6 ₃ /mmc	[Landolt '08]
Cu _{1.93-ϵ} S	Djurlite	T ≤ 100 °C	1.93-1.97 at 72 °C	Pmmm, P2 ₁ nm or Pmn2 ₁	[Massalski '90], [Landolt '08]
Cu _{1.75} S	Anilite	T ≤ 39 °C	1.75	Pnma	[Landolt '08]
Cu _{2-δ} S	Digenite	52 °C ≤ T ≤ 1403 °C	1.76-1.81 at 80 °C	Fm-3m	[Massalski '90]

The In-S Material System

The binary phase diagram of the In-S material system is shown in Appendix IV (Fig. IV.2). In this system, numerous stable phases exist including high-temperature and high-pressure phases [Massalski '90]. At room temperature and normal pressure (1013 mbar), InS, In₆S₇ and In₂S₃ are stable [Massalski '90]. In₂S₃ exists in two different modifications (α -In₂S₃ and β -In₂S₃); note that the nomenclature in the literature is inconsistent. In the course of this thesis the compound exhibiting a defect spinel structure (Space group I41/amd) will be referred to as α -In₂S₃, according to Ref. [Massalski '90]. In contrast β -In₂S₃ has a cubic structure and belongs to the space group Fd-3m. α -In₂S₃ is the only stable In₂S₃-phase at room temperature, even though the metastable β -In₂S₃ can also be observed at room temperature [Kambas '81]. The unit cell of α -In₂S₃ contains 16 atoms, with indium occupying all octahedral sites as well as 2/3 of the tetrahedral metal positions of the spinel lattice. 1/3 of the tetrahedral metal positions remain empty. These empty sites are ordered in a screw axis by alignment of three spinel blocks along the c-axis of the crystal. In β -In₂S₃, the empty sites are randomly distributed [Kambas '81]. Hence, α -In₂S₃ can be regarded as a quasiternary spinel compound AB₂X₄ of the composition (In_{0.66}□_{0.33})In₂S₄, where □ denotes an indium vacancy. All listed indium sulfide compounds are indirect n-type semiconductors [Landolt '08]. In Table 2.3, the stability ranges, [In]:[S] ratios and space groups of the discussed phases are listed.

Table 2.3: Stable indium sulfide phases in the In-S material system at normal pressure (1013 mbar) for the relevant temperature range of this thesis ($25\text{ °C} \leq T \leq 550\text{ °C}$). The stability range, [In]:[S] ratio and space group are listed for each phase.

	Stability Range at 1013 mbar	[In]:[S]	Space group	Reference
InS	$-200\text{ °C} \leq T \leq 660\text{ °C}$	1.05	Pnnm	[Massalski '90], [Qasrawi '02]
In ₆ S ₇	$-200\text{ °C} \leq T \leq 759\text{ °C}$	0.86	P2 ₁ /m	[Massalski '90], [Gamal '97]
α -In ₂ S ₃	$-200\text{ °C} \leq T \leq 414\text{ °C}$ (varies with [In]:[S] ratio)	0.67-0.69	I4 ₁ /amd	[Massalski '90], [Kambas '81]
β -In ₂ S ₃	$-200\text{ °C} \leq T \leq 852\text{ °C}$	0.67-0.72	Fd-3m	[Massalski '90], [Pejova '06]

The In-O Material System

No phase diagram of the binary system In-O is known [Massalski '90]. However, In₂O, InO and In₂O₃ are known to exist in this system, In₂O₃ being the compound most frequently observed [Massalski '90] at room temperature and normal pressure (1013 mbar). In₂O₃ has a cubic body-centered structure of space group Ia-3 [Massalski '90]. Due to the complicated electronic band structure of In₂O₃ the nature of its band gap is still under discussion. An indirect band gap of 2.1-2.7 eV as well as a direct band gap of about 3.6 eV have been reported [Hamberg '86; Klein '00; Erhart '07]. The conductivity of In₂O₃ has been determined to be n-type, which can be explained by the generation of shallow donor levels by indium atoms, which occupy interstitial lattice sites [Tomita '05]. By doping with tin the highly conductive ITO (In₂O₃:Sn) can be prepared, which is a commonly used transparent conducting oxide [Hamberg '86]. Additionally to the cubic In₂O₃, also a metastable rhombohedral In₂O₃ phase of space group R-3c has been observed at room temperature and normal pressure [Massalski '90].

2.2. Deposition Methods for Chalcopyrite Thin Films

In this section, a brief overview of methods for the deposition of chalcopyrite thin films is given. The most relevant and established methods are discussed. Besides these, also non-vacuum processes aiming for low-cost deposition are mentioned. A special emphasis will be given to spray pyrolysis and atomic layer deposition, since both are related to the Spray ILGAR process. For further information about these deposition methods the reader is referred to Ref. [Schock '96; Lux-Steiner '00; Romeo '04], [Winkler '01; Kaelin '04; Lincot '04; Winkler '04; Kaelin '05] and [Tomar '81; Mooney '82; Bougnot '86; Mooney '86; Reijnen '03; Perednis '05; Nanu '06], respectively.

Co-Evaporation of the Elements

To date, the most-efficient chalcopyrite thin-film solar cells with efficiencies of up to 19.9 % consist of Cu(In,Ga)Se₂ and are prepared by simultaneous evaporation of the elements in a three-stage-process using physical vapor deposition (PVD) [Repins_1 '08]. Also, the first CuInS₂-based solar cells reaching efficiencies above 10 % have been prepared by PVD [Scheer '93]. In PVD-processes the different elements are evaporated at temperatures around 1000 °C under vacuum and deposited onto a heated and rotating substrate. The evaporation rates of the different elements can be controlled separately. Thus, a very precise process and composition control is possible, which is responsible for the high quality of the material. However, due to the high evaporation temperatures and the high vacuum, such processes are a rather expensive way for producing chalcopyrite solar cell absorbers, which limits their applicability for industrial production.

Sequential Processes

Another well-established group of processes are the sequential deposition processes, in which metallic precursor layers are heated in a chalcogen-containing (sulfur or selenium) atmosphere. Upon heating, the metals react with the chalcogen, yielding the chalcopyrite phase. Besides sulfur or selenium, H_2Se or H_2S gas can also be used. The metallic precursor layers can be deposited by various methods: sputtering, electrodeposition and PVD have all been successfully applied in sequential processes.

One of these processes - the *baseline-process* for $CuInS_2$, which was developed at the Hahn-Meitner-Institut - is subsequently briefly described. $CuInS_2$ thin films from the baseline-process served as reference material in the course of this thesis. For a detailed description of this process refer to Ref. [Klaer '98; Siemer '01; Klaer '03].

The process starts by sputtering the molybdenum back contact (thickness: about 1 μm) onto the substrate. This is followed by the sputtering of copper and indium layers ($[Cu]:[In] = 1.8$). These layers are sulfurized in elemental sulfur vapor, resulting in single-phase chalcopyrite $CuInS_2$ covered by a CuS layer. The sulfurization is performed at a heating rate of 3 $^{\circ}C/s$ up to a temperature of 580 $^{\circ}C$, which is held constant for 60 s before the sample cools down to room temperature. This heating in sulfur atmosphere is referred to as "*rapid thermal processing*" (RTP). The covering CuS layer is removed by etching the films in a KCN solution [Scheer '95; Weber '02]. If these $CuInS_2$ thin films are further processed to solar cells, the KCN etching is followed by the deposition of a CdS buffer layer (50 nm) in a chemical bath and sputtering of a ZnO window layer (400 nm). Finally, the solar cells are completed by the deposition of Ni/Al-front contacts. The best efficiency of 11.4 % reported for a $CuInS_2$ -based solar cell to date was achieved for a solar cell which was prepared in the baseline-process [Siemer '01]. Besides yielding high efficiencies, the baseline-process is also highly reproducible [Klaer '07]. In the following, these thin films will be referred to as "*RTP- $CuInS_2$* ".

Due to its simplicity and reproducibility, this process is already applied industrially [Meyer '07]. Even though $CuInS_2$ -based solar cells are less efficient than $Cu(In,Ga)Se_2$ solar cells, the application of this material is still attractive, since the modules prepared from the baseline process reach efficiencies of up to 11 % [Klaer '07], which almost match those of the best solar cells, whereas for other materials the difference between cell and module efficiencies is more pronounced.

Preparation Methods for Single-crystalline and Epitaxial Materials

Another important group of deposition methods for chalcopyrite thin films are metal organic chemical vapor deposition and molecular beam epitaxy, which are both capable of depositing epitaxial thin films on single-crystalline substrates [Artaud-Gillet '03], [Hunger '96]. However, both methods are very slow and expensive and are thus mainly used for the preparation of reference material for research applications. The same is true for chemical vapor transport (CVT), which is a common method for the preparation of bulk chalcopyrite single crystals [Tomm '05]. Such single crystals are a very important prerequisite for basic materials research.

Spray Pyrolysis

Spray pyrolysis is a non-vacuum low-cost method, which has been applied for the deposition of chalcopyrite thin films. First reports on the deposition of $CuInSe_2$ and $CuInS_2$ thin films by spray pyrolysis date back to the late seventies and early eighties [Gorska '79; Pamplin '79; Bates '82; Bates '83; Gabor '94]. In spray pyrolysis of $CuInS_2$, a solution (mostly aqueous) of

copper and indium salts (mostly chlorides) and thiourea as a sulfur source is sprayed onto a heated substrate. Due to the elevated substrate temperature, CuInS_2 is formed as soon as the thiourea decomposes. However, even though the method of spray pyrolysis is well established, only very few reports exist about solar cells processed from thin films which have been deposited by spray pyrolysis, exist. The best efficiency reported by Duchemin *et al.* for a sprayed CdS-CuInSe_2 solar cell was about 5 % in 1989 [Duchemin '89]. Most probably the low conversion efficiencies achieved by this technique are mainly due to the high impurity content and the small grain sizes observed in such thin films, even though it has been shown that the grain size can be increased by post-deposition treatments [Krunks '02; Krunks '06].

Other Non-vacuum Processes

Besides the vacuum-based deposition methods for the preparation of chalcopyrite thin films, also numerous alternative non-vacuum processes have been presented, which potentially allow for low-cost fabrication of chalcopyrite-based thin-film solar cells. In the following some of these processes are briefly described. A detailed review on low-cost processes for chalcopyrite thin film deposition is given in Ref. [Kaelin '04].

Lincot *et al.* obtained an efficiency of 11.3 % for solar cells based on electrodeposited Cu(In,Ga)Se_2 [Lincot '04]. Winkler *et al.* introduced the CISCuT process, in which CuInS_2 is deposited onto a flexible copper tape [Winkler '04]. In this process, indium and copper are deposited by electrodeposition and sulfurized subsequently. Efficiencies of 9 % for CISCuT solar cells have been achieved. The highest efficiencies of chalcopyrite-based thin-film solar cells using low-cost deposition processes have been obtained in the ISET-process by Kapur *et al.* [Kapur '01]. Here, an ink of copper oxide, indium oxide and gallium oxide nanoparticles is deposited onto a molybdenum-coated substrate. This precursor layer is reduced by H_2 and selenized by H_2Se , yielding Cu(In,Ga)Se_2 . Solar cells processed from these thin films, have reached efficiencies of up to 13.6 % [Kapur '03].

Atomic Layer Deposition

Atomic layer deposition (ALD) or atomic layer epitaxy is a cyclic vacuum-based method for the deposition of semiconductor thin films. For the deposition of sulfides, a monolayer of a metal-organic precursor compound is deposited onto the sample in short pulses of 100-300 ms by a carrier gas stream. Subsequently, this layer is converted to sulfide by H_2S . Due to the monolayer-growth mode, this method leads to very homogeneous thin films, which adhere well to the substrate. However, this method is very slow and not applicable for industrial deposition of solar cell absorber layers of a thickness of several μm , even though it has been demonstrated that CuInS_2 thin films can be deposited by ALD [Reijnen '03; Nanu '04; Nanu '06]. Therefore, this process is rather used for the deposition of buffer layers in thin-film solar cells. This has been successfully demonstrated by Platzer-Björkman *et al.* [Platzer-Björkman '06] for Zn(O,S) buffer layers and by Naghavi *et al.* [Naghavi '03] for In_2S_3 . The reaction principle of the ALD process is very similar to the principle underlying the Spray ILGAR-process, which is the focus of this thesis.

2.3. The “Ion Layer Gas Reaction”

The “Ion Layer Gas Reaction” (ILGAR) method, which is the focus of the present work, is discussed in the following. The main characteristics, as well as the various modifications of this deposition technique which have been used to date, are reviewed in view of the challenge of applying this process for the fabrication of CuInS_2 thin films. Additionally, advantages and relations to previously described methods are highlighted.

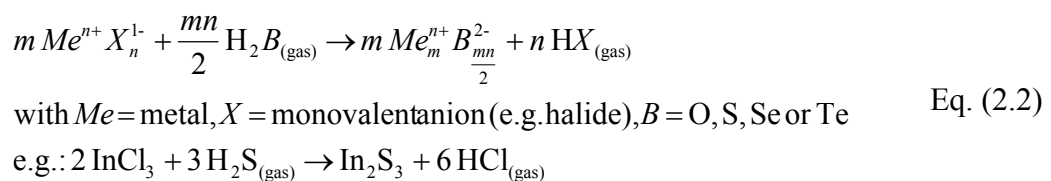
In this thesis, the ILGAR process is used for the deposition of CuInS₂ thin films, which are meant to be used as absorber layers in planar thin-film solar cells. Even though it is not a goal of this thesis to develop a fully optimized industrial process, the deposition of the CuInS₂ thin films must be possible within reasonable process times, whilst a high material quality is still ensured. A *deposition time of 1-2 hours for a 2 μm thick absorber layer* was regarded to be acceptable for a novel deposition technique. This corresponds to a *deposition rate of about 20-30 nm per minute*. In order to be able to deposit all layers of a chalcopyrite thin-film solar cell, it is desirable to set up a process that is principally capable of depositing absorber films and window layers as well as buffer layers. Therefore, the deposition rate of the process should be tunable over a range from about 1-3 nm per minute for buffer layer deposition to 20-30 nm per minute for the deposition of the window layer or the absorber film. Hence, in the following discussion of the ILGAR process, a special emphasis is placed on the deposition rates that have been achieved with the various setups to date.

The ILGAR process was developed at the Hahn-Meitner-Institut in Berlin and is protected by several patents [Patent1; Patent2]. Initially the method was introduced as a coating method for the deposition of compound semiconductors on highly porous substrates [Möller '00]. The method was then successfully used for the deposition of metal oxide [Bär '01] and sulfide [Muffler '01] thin films. Both kinds of thin films play an important role in chalcopyrite solar cells: metal sulfide thin films, such as CuInS₂ or CdS and In₂S₃, can be used as absorber layers or buffer layers, respectively (section 6.1.). Metal oxide layers, such as ZnO, are used as window layers in chalcopyrite solar cells. Thus, in principle, all parts of a chalcopyrite solar cell, apart from the molybdenum back contact, can be deposited by the ILGAR method. Furthermore, the ILGAR method is a non-vacuum deposition method and could therefore contribute to a cost reduction in the production process of thin-film solar cells.

The ILGAR process consists of three separate steps, which are explained in the following:

- Firstly, a precursor solution consisting of a metal salt (e.g. InCl₃) dissolved in a solvent (e.g. ethanol) is deposited (either by dipping or spraying) onto a substrate from a precursor solution.
- Secondly, the solvent evaporates, leaving a solid precursor layer on the substrate. Depending on the porosity of the substrate and the volatility of the solvent, this step either can take place by itself or must be carried out actively by an additional drying step, in which the substrate is heated in a nitrogen atmosphere. If the substrate is heated continuously, the first and second step can take place simultaneously.
- Finally, the precursor film is converted into the desired compound semiconductor (e.g. In₂S₃) by an appropriate reactant gas at a suitable temperature. In the case of sulfide deposition, H₂S is used as a reactant gas. For the deposition of oxides, ammonia-enriched H₂O is used. In the latter case, the oxide is not formed directly, but via a hydroxide, which is subsequently dehydrated to the corresponding oxide.

These steps, which constitute one ILGAR-cycle, are cyclically repeated until the desired layer thickness is achieved. The chemical reaction path of the ILGAR process can be summarized in the following equation:



Since the ILGAR method has been introduced in the year 2000, the original setup used for the deposition was modified in order to improve the homogeneity of the deposited layers and to reduce deposition times. In the following, three different modifications of the ILGAR process that have been used in the past are discussed.

Dip ILGAR

Originally, the precursor solution was deposited onto the substrate by dipping it into the solution (“dip ILGAR”) [Möller '00]. The dip ILGAR process is schematically shown in Fig. 2.6 for the case of In_2S_3 deposition from an InCl_3 solution.

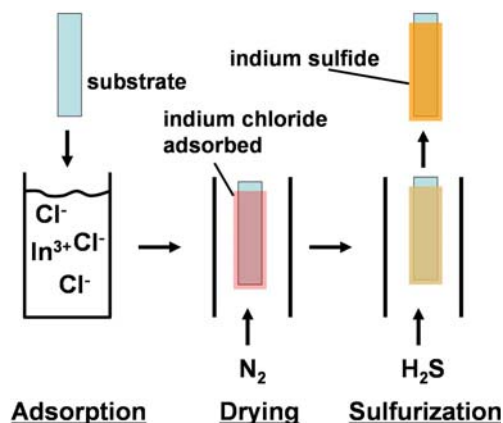


Fig. 2.6: Schematic sketch of the dip ILGAR setup for deposition of In_2S_3 from an InCl_3 solution.

Firstly, the substrate is dipped into the InCl_3 solution, which leads to wetting of the substrate with the solution. In the next step, the sample is dried in a nitrogen atmosphere. Thereby, the solvent evaporates and a solid InCl_3 layer remains on the substrate. Subsequently, this layer is converted to In_2S_3 by H_2S in a separate reaction chamber.

Since the dip ILGAR method proved to be able to homogeneously coat even highly porous TiO_2 substrates [Möller '00], it is also well-suited for coating the rough surface of chalcopyrite absorber films. Therefore, it could be successfully used for the deposition of various buffer layers, such as ZnS , CdS [Muffler '01] and $\text{Zn}(\text{O},\text{OH})$ [Bär '02] in chalcopyrite-based thin-film solar cells.

The deposition rate of the dip ILGAR process is about 0.5-1.5 nm per minute [Muffler '01]. Since buffer layers are only about 20-50 nm thick (section 6.1.), a deposition rate in the range of a few nanometers per minute for these layers can be tolerated. However, due to the low deposition rate, this process can not be transferred to a deposition process for CuInS_2 absorber films for planar thin-film solar cells, which have a thickness of about 2 μm (section 6.1.). For a deposition rate of 1 nm per 50 seconds [Bär '02], the deposition of the absorber film would require about 28 hours.

Spray ILGAR I

In a first approach to increase the deposition rate, an ILGAR setup was developed in which an aqueous metal chloride solution was sprayed onto a moderately ($T_{\text{sub}} = 65\text{-}100\text{ }^\circ\text{C}$) heated substrate [Fischer '03]. This setup is shown in Fig 2.7.

Here, an aerosol is formed from the solution by a pneumatic nebulizer. The droplets of this aerosol are transported by a nitrogen carrier gas stream and arrive vertically at the substrate. While the residual water evaporates from these droplets the precursor salt recrystallizes on the surface and thereby forms a solid layer. In the next process step, this layer is sulfurized by a suitable reactant gas as in the dip ILGAR process. With this setup, 2 μm thick CuInS_2 thin films have been deposited with deposition rates of 30-60 nm per minute. After an additional post-deposition annealing step in hydrogen sulfide (H_2S) atmosphere, solar cells yielding 1.7 % efficiency have been processed from such thin films [Fischer '03].

Even though the deposition rates obtained with this setup are in the desired range it did not allow for the deposition of well-crystallized material for several reasons: The pneumatic nebulizer produces droplets of an average diameter of about 10 μm . Due to the setup geometry, the use of a non-volatile solvent (H_2O) and the moderate substrate temperature,

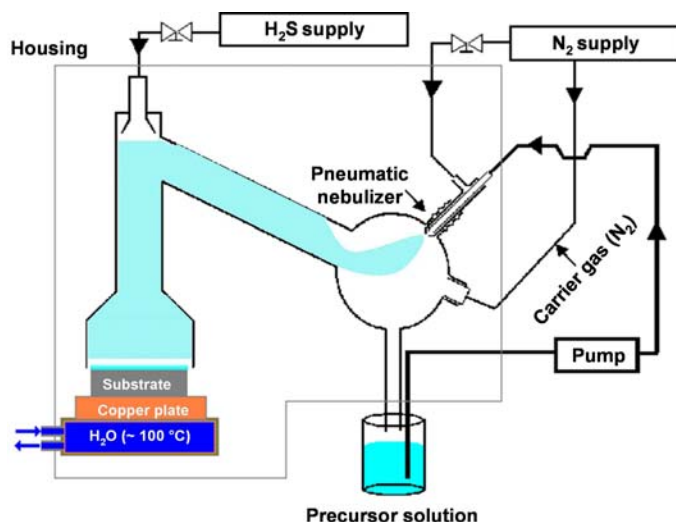


Fig. 2.7: Schematic sketch of the first Spray ILGAR setup for compound semiconductor thin film deposition. The image was redrawn from Ref. [Kropp '02].

these droplets reach the substrate surface in the liquid state. This leads to an inhomogeneous deposition, which prevents the formation of well-crystallized material even after an additional post-deposition annealing. Furthermore, this setup also did not allow for the deposition of thin and smooth layers as are needed for the deposition of buffer layers.

Spray ILGAR II

In order to improve the homogeneity of the deposited films, the Spray ILGAR setup was redesigned by Allsop *et al.* [Allsop_1 '05; Allsop_1 '06] so that the aerosol droplets did not impinge vertically onto the substrate (Fig. 2.8). This was achieved by tilting the sample to an angle of 45 °, so that the aerosol can pass the substrate and turbulences are reduced. Additionally, the aqueous solution was replaced by a more volatile ethanol solution and the substrate temperature was increased to about 250 °C, which led to a more complete evaporation of the aerosol droplets in the vicinity of the substrate surface. Finally, the pneumatic nebulizer was replaced by an ultrasonic source (1.65 MHz), which produces a much finer mist (mean droplet size 2 μm). In Fig. 2.8, a schematic sketch (Fig 2.8a) and a photograph (Fig. 2.8b) of this Spray ILGAR setup are shown.

In this setup, an InCl₃/ethanol solution is nebulized by the ultrasonic source. Afterwards the aerosol is transported by a nitrogen carrier gas stream to the heated substrate. Close to the substrate, the solvent evaporates from the aerosol droplets and a solid precursor layer is deposited onto the surface. In contrast to the ILGAR setups shown in Fig. 2.6 and 2.7, this layer is not deposited by a pure adsorption process, but by a chemical surface reaction, which is due to the elevated substrate temperature of about 250 °C. Therefore, the solid precursor layer does not consist of InCl₃ but of an indium hydroxide chloride compound In_x(OH)_yCl_z ($x = 1 \pm 0.1$; $y = 1.6 \pm 0.1$; $z = 1 \pm 0.1$), which results from a chemical reaction of InCl₃ and ethanol [Allsop_1 '06]. The surface temperature of the substrate is passively reduced during the spray step due to the cooling effect of the evaporating aerosol droplets [Paap '06]. The extent of this cooling is in the range of several °C: Paap found a temperature reduction of up to 20 °C for water aerosol. For volatile solvents the effect can be expected to be smaller, since the heat of evaporation is smaller (H₂O: 2256 kJ/kg, ethanol: 904 kJ/kg) [Paap '06]. In the next process step the precursor layer is converted into its corresponding sulfide by hydrogen sulfide (H₂S) gas. These two steps are then cyclically repeated until the desired film thickness is achieved. Fig. 2.9 depicts the Spray ILGAR deposition process schematically: In Fig. 2.9a, the solid In_x(OH)_yCl_z layer is deposited as a solid precursor layer from the InCl₃/ethanol aerosol onto the heated substrate. This layer is then converted to In₂S₃ by H₂S (Fig. 2.9b and c). By repeating this cycle for an appropriate number of times in principle any desired layer thickness can be achieved.

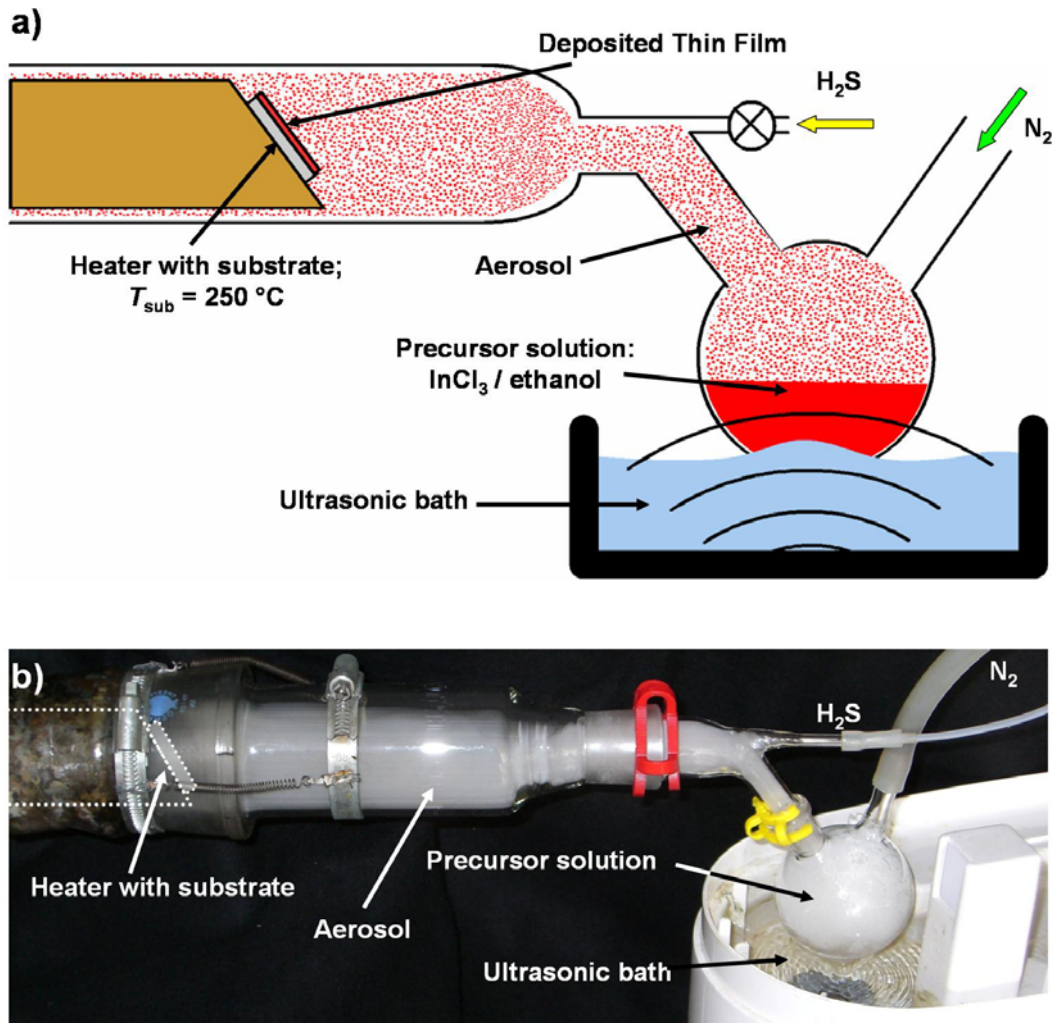


Fig. 2.8: a) Schematic sketch of the Spray ILGAR setup used by Allsop *et al.* for the deposition of Spray ILGAR In_2S_3 thin films; redrawn from [Allsop_1 '06]. b) Photograph of the same setup during nebulization of the precursor solution ($\text{InCl}_3/\text{ethanol}$).

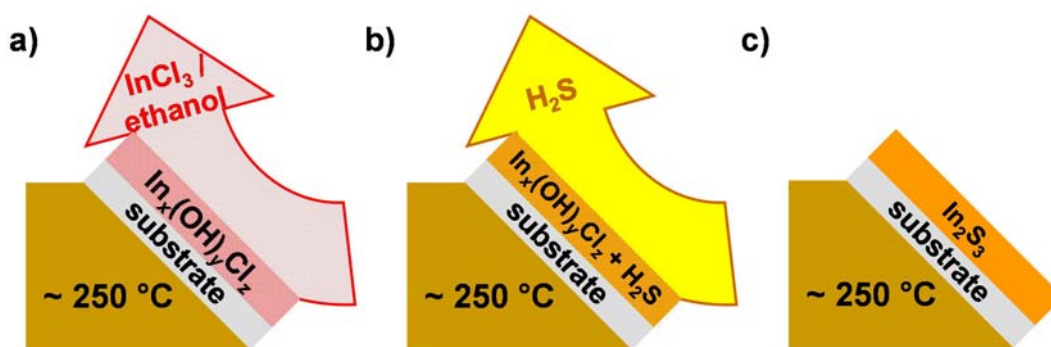


Fig. 2.9: Schematic sketch of the ILGAR mechanism for the deposition of In_2S_3 thin films from an InCl_3 / ethanol solution as it was established by Allsop *et al.* [Allsop_1 '06]: a) a solid $\text{In}_x(\text{OH})_y\text{Cl}_z$ layer is deposited from an InCl_3 / ethanol aerosol; b) to c) conversion of this layer to In_2S_3 by H_2S . This sketch is simplified in respect that the deposited layer is not yet closed after one single cycle but rather consists of islands, which are scattered over the substrate surface. After 2-3 cycles a complete coverage of the surface of the substrate is achieved [Allsop_1 '06].

In combination, the modifications led to a fundamental change of the deposition process. In Ref. [Allsop_1 '06] it was shown that the deposition of the precursor material with this setup takes place from the vapor phase. This is a direct consequence of the more pronounced

temperature gradient close to the substrate as well as of the smaller droplet size of the nebulized precursor mist: The smaller droplet size increases the surface-to-mass ratio of the droplets, which enhances the evaporation of the droplets. Furthermore, the elevated substrate temperature as well as the stronger temperature gradient lead to the build-up of a so-called *thermophoretic force* [Perednis '05; Allsop_1 '06]. This force is due to the different temperatures of a surrounding gas on the two sides of a specific droplet which is located in a temperature gradient. This difference in temperature leads to a net force, which hinders the transport of this droplet towards the hot surface that causes the temperature gradient². Thus, a larger portion of the precursor solution droplet can evaporate and deposit from the vapor phase. Due to this much smoother deposition process compared to the former Spray ILGAR setup (Fig. 2.7), the homogeneity of the deposited thin films could be improved.

In this modification (Fig. 2.8), the Spray ILGAR method is related to both ALD and spray pyrolysis (section 2.2.). The experimental setup is rather similar to a spray pyrolysis setup and also the deposition of the solid precursor layer can be understood as spray pyrolysis process. In contrast, the cyclic processing and the resulting growth mechanism (Fig. 2.9) are more similar to ALD.

With this modified Spray ILGAR setup (Fig. 2.8), Allsop *et al.* deposited In₂S₃ buffer layers for highly efficient Cu(In,Ga)(S,Se)₂ thin-film solar cells [Allsop_1 '05; Allsop_1 '06; Allsop_2 '06]. The deposition process also allowed the deposition of nanostructured ZnS:In₂S₃ buffer layers, which further improved the conversion efficiency of such devices [Allsop '07]. The durations of the single steps in the ILGAR-cycle and the experimental parameters for the In₂S₃ thin film deposition, which were optimized empirically by Allsop *et al.* with respect to solar cell efficiency, are listed in Table 2.4 [Allsop_1 '06].

Table 2.4: Sequence of the different process steps of one ILGAR-cycle as it was used for the deposition for Spray ILGAR In₂S₃ buffer layers in Cu(In,Ga)(Se,S)₂-based thin-film solar cells.

Step	Duration [sec]	Process
1	60	Spraying: deposition of In _x (OH) _y Cl _z layer
2	10	Pause: Purging of Reactor
3	20	H ₂ S gassing: Sulfurization of In _x (OH) _y Cl _z layer
4	10	Pause: Purging of Reactor

These conditions were found empirically by Allsop *et al.* by optimizing the efficiency of the solar cells. The substrate temperature of 250 °C was held constant during the entire process. The nitrogen carrier gas flow was also fixed at 5.5 l/min and the flow rate of H₂S was set to 1.3 l/min. A 25 mM InCl₃/ethanol solution was used for the deposition. An optimum efficiency was found for a buffer deposition process, which consisted of seven ILGAR-cycles [Allsop_1 '05; Allsop_1 '06].

The deposition rate of this modified setup was in the range of about 4 nm per minute [Allsop_1 '06], which is below the desired rate for the deposition for CuInS₂ absorber layers of a thickness of 1-2 μm. However, in Ref. [Allsop_1 '06] it was shown that this rate could be doubled by increasing the substrate temperature. Besides temperature, the setup shown in Fig. 2.8 also allows other parameters, such as the nitrogen flow rate or the choice of solvents and metal compounds, to be changed. Hence, a modification of this setup in order to increase the deposition rate seems possible.

Preliminary experiments on the deposition of copper sulfide thin films from ethanol solutions were also performed by Allsop with various copper compounds (CuCl, CuCl₂, Cu(NO₃)₂ and copper acetate) using the setup shown in Fig. 2.8 [Allsop_2 '05]. In all these experiments, the

² Perednis *et al.* calculated that, for H₂O, the thermophoretic force equals the gravitational force for a droplet of 2 μm in diameter, which approaches a surface with a surface temperature of 350 °C in a thermal gradient of 500 °C/cm [Perednis '05].

deposition rates were well below 1 nm per minute and thus these solutions were regarded not to be suitable for the deposition of absorber films.

This shows that besides the deposition rate, more fundamental changes of the Spray ILGAR process might be necessary in order to design a process for the deposition of CuInS_2 solar cell absorber layers. The realization of such a process is the main topic of this thesis.

